2009

CFD analysis of air turbines as power take-off systems in oscillating water column wave energy conversion plant

Andrei Gareev
University of Wollongong, ag839@uow.edu.au

Paul Cooper
University of Wollongong, pcooper@uow.edu.au

Kosasih
University of Wollongong, buyung@uow.edu.au

CFD Analysis of Air Turbines as Power Take-Off Systems in Oscillating Water Column Wave Energy Conversion Plant

A. Gareev, P. Cooper and P. B. Kosasih

School of Mechanical, Materials and Mechatronic Engineering,
University of Wollongong, Wollongong, NSW 2522, AUSTRALIA.
e-mail: pcooper@uow.edu.au

Abstract

This paper presents the results of CFD simulations of reversing flow air turbines used as the power take-off system in Oscillating Water Column (OWC) Wave Energy Conversion (WEC) plant. One of the simpler tools to analyse such turbines is the blade element/actuator disc methodology. This requires the input of "interference factors" to model how the lift and drag characteristics of the cascade of blades on the turbine rotor are related to those of a single isolated aerofoil. In the first part of the paper, CFD modelling to obtain the lift and drag characteristics of various aerofoils arranged in linear cascades at different stagger angles is described. The CFD cascade lift and drag data are compared with reported experimental cascade aerodynamic data. The agreement within the range of usable stagger angles is excellent in the pre-stall range with some deviations shown in the post-stall. A comparison is also made between our 2D CFD interference factors and those previously reported by Weinig and others who used analytical, inviscid flow theory. It is found that the Weinig inviscid flow theory provides a reasonable prediction of the lift interference factor providing that both the angle of attack is relatively low and that the thickness of the blades is relatively small compared to the distance between blades. In the second part of the paper, three-dimensional simulations of a Wells air turbine rotor using CFD unstructured and structured grid designs are described. The results of the three-dimensional CFD simulations were then compared with those from our non-dimensional blade element model incorporating the linear cascade aerodynamic data described in the first part of the paper. The two sets of results are compared in terms of torque coefficient and pressure coefficient.

Keywords: air turbine, blade element, computational fluid dynamics , cascade, aerofoils, variable pitch, wave energy

Nomenclature

a' = tangential flow induction factor, $V_\theta/(\Omega R)$
b = blade span
c = chord length of the blade
C_a = input coefficient
C_D = drag coefficient
C_{D0} = drag coefficient for an isolated airfoil
C_L = lift coefficient
C_{L0} = lift coefficient for an isolated airfoil
C_t = torque coefficient
C_ϕ = blade axial coefficient
C_θ = blade tangential coefficient
k_0 = interference factor for lift (C_L/C_{L0})
N = number of blades
P^* = pressure coefficient
R = radius
R_t = radius of blade tip
R_{av} = mean radius of the blade
R_r = hub radius
s = blade spacing
V_z = axial velocity at the blade
V_θ = tangential velocity at the blade
W = resultant relative velocity on the blade
α = angle of attack ($\beta - \gamma$)
β = angle of relative velocity to plane of rotor
δ_0 = interference factor for drag (C_D/C_{D0})
ϕ = flow factor (V_z/V_θ)
γ = blade pitch (stagger) angle
η = turbine efficiency
ρ = density of air
σ = solidity= c/s
Ω = angular velocity

1 Introduction

The overall capture efficiency of any OWC WEC is critically dependent on the performance of the air turbine used to extract mechanical energy from the air flow generated by the moving free surface in the OWC chamber (Fig. 1). The air turbine must be of high efficiency over a wide range of air flow velocities and it must also provide the optimum pneumatic damping required to ensure maximum hydrodynamic capture efficiency of the OWC *per se*.

Relatively few full-scale OWC turbine systems have been designed and tested to date. Examples include the Limpet on the Isle of Islay in the UK [1], the Pico plant in the Azores [2] and the Oceanlinx plant at Port Kembla, just south of Wollongong, in New South Wales, Australia [3]. The oscillating and bi-directional airflow through the air turbine provides a major challenge to the designer who must accommodate a number of conflicting requirements such as the need to optimise the angle of attack on the rotor blades for maximum power output while maintaining the required pressure drop through the turbine. To date the most common form of turbine implemented in practice has been the Wells turbine [4], in various configurations (eg fixed blade pitch, with and without guide vanes, multi-stage, etc). Other variable blade pitch angle

rotors have also been trialled, such as the Dennis-Auld turbine [5], as well as impulse turbines. The OWC chamber itself requires a certain "pneumatic damping" to provide the optimal wave energy hydrodynamic efficiency (see for example Thomas [6]). Thus, one of the main turbine design issues that must receive particular attention is the need to provide the required pressure drop over the wide range of flow conditions that can arise throughout each wave cycle.

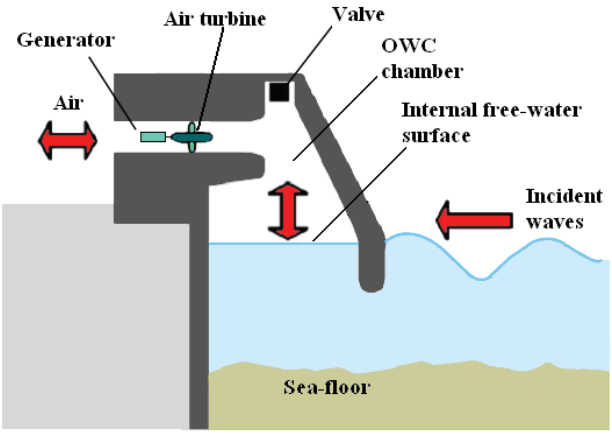

Figure 1: Schematic of Wave Energy Conversion based on an Oscillating Water Column (OWC) device.

One of the main aims of the research by the present authors is to develop a coherent and comprehensive methodology for designing and optimizing of the air turbines suitable to service OWC systems. In this paper we present our recent fundamental Computational Fluid Dynamics (CFD) research on the lift and drag characteristics of linear cascade aerofoils and aerodynamic behaviour of flow through OWC air turbine rotors without guide vanes with either fixed or variable pitch blades.

2 Analysis of Linear Aerofoil Cascades and Interference Factors

As with the design of wind turbines, the most common starting point for the analysis of rotors such as the Wells Turbine is the blade element/actuator disc methodology. Prior to the development of this methodology the analysis of axial flow turbines was carried out by applying methods based on the knowledge of the aerodynamics of "cascades", which involved a number of assumptions regarding the flow through the rotor and a great deal of empirical data (see Dixon [7], for example).

One of the difficulties of the blade element model is that in a relatively high solidity rotor, as is common in many OWC air turbines, the interference between the blades in the circular cascade of blades is not known *a priori*. It is also true that fundamental experimental testing of a cascade of aerofoils at high stagger (or pitch) angles, γ, (see Fig. 2) is virtually impossible in a wind tunnel [8]. In the past the interference of adjacent blades in a cascade at various stagger angles has been estimated by a number of methods including: i) potential flow analysis of flat plate aerofoils arranged in a straight-line cascade as proposed by Weinig [9] and the Method of Singularities [10]. It should be noted that both these inviscid theoretical methods make it possible to estimate cascade lift coefficients, but not the drag values. A third approach reported is a semi-empirical method based on a correlation between computed values of mean aerodynamic force coefficients from a turbine test and 2D aerofoils data obtained in a wind tunnel [10].

Hawthorne and Horlock [11] and others in the 1960's pioneered the actuator disk/blade element method to determine turbine performance in a similar manner to the analysis of un-ducted fans and turbines such as wind turbines. The blade element/actuator disc methodology in a ducted turbine provides a means to determine the swirl velocity downstream of the rotor and using lift/drag data for the blade profiles, the forces are calculated and hence the pressure drops across device as well as other important turbine performance characteristics (C_l, C_a and η) are determined. Some of the first researchers to apply the actuator disc methodology to the analysis of the Wells turbine were Gato and Falcão [12].

Today CFD may be used to obtain 2D cascade aerodynamic coefficients at any stagger angle as well as to simulate the details of complex 3D airflow through the axial turbine. However, the blade element/actuator disc analysis remains the key tool for the conceptual stage of turbine design when the designer needs to obtain a quick and reasonably accurate estimation of the turbine performance and to determine the possible ways to optimise the configuration of a turbine with respect to parameters such as radius, flowrates, rotational speed, etc.

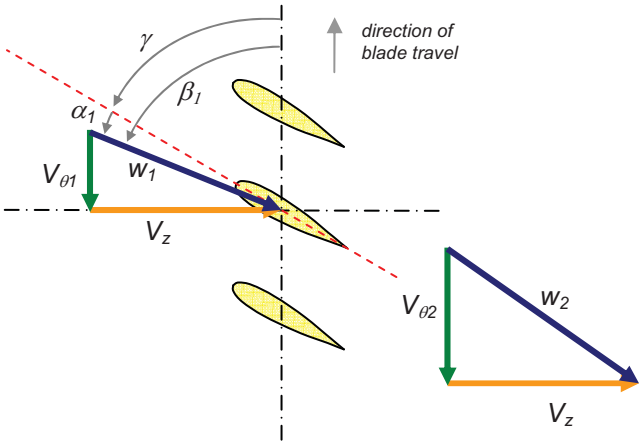

Figure 2: Nomenclature for a cascade of aerofoils with stagger angle, γ, on an axial flow turbine rotor, with axial air velocity, V_z, and tangential velocity relative to aerofoils, V_θ.

Accurate prediction of turbine performance parameters using the blade element/actuator disc methodology requires the input of reliable lift and drag data for blades arranged in a cascade, as shown in Fig. 2. Relatively little fundamental research has been published on the flow in such rotors until recently. In the sections below we present an outline of the

theoretical results of Weinig [10] that have been used by several researchers to modify the isolated aerofoils lift coefficient so as to be applicable to the analysis of cascades, and we compare Weinig's theory with our CFD results.

We consider an infinite and linear cascade of aerofoils of a given arbitrary shape as shown in Fig. 2. The aerofoils interact with each other and the lift and drag coefficients are no longer the same as for a single isolated aerofoil. The ratio of the lift coefficient of a blade in a cascade, C_L, relative to that of an isolated blade, C_{L0}, is known as the "interference factor", $k_0 = C_L/C_{L0}$.

As mentioned above, testing of aerofoil cascades to determine k_0 is difficult. Only a very few, small, data-sets applicable to turbines used in OWC applications are available in the public domain (eg Ragunathan [10]). Thus, most, if not all, researchers analysing the Wells turbine have relied on the earlier work of Weinig [10] who determined an analytical prediction of the interference factor for a linear cascade of infinitesimally thin flat blades using potential flow theory.

Weinig's results showed that the interference factor is independent of the angle of incidence, $\alpha = \beta - \gamma$, and is a function only of the stagger angle, γ, and solidity, $\sigma = c/s$ (where c is the blade chord length and s is the blade pitch, eg distance from leading edge to leading edge of adjacent blades). A key graph from Weinig's paper is reproduced in Fig. 3.

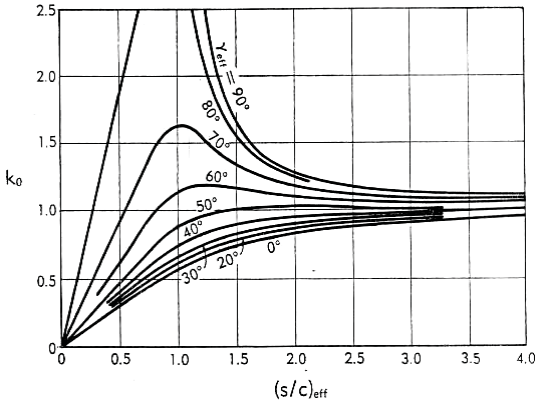

Figure 3: Prediction of the interference factor, $k_0 = C_L/C_{L0}$, from potential flow theory [9]. $\gamma_{eff} = 90^o - \gamma$.

For the general case of a cascade with arbitrary solidity and stagger angle Weinig's inviscid flow analysis provides the following estimate of lift coefficient for an isolated aerofoil prior to stall modified by the interference factor, k_0:

$$C_L = 2\pi k_0 \sin(\alpha_m) \qquad (1)$$

Where α_m is the angle of attack (based on the mean of the velocities upstream and downstream of the cascade) and where k_0 (shown in Fig. 3) was found through the solution of a set of algebraic equations [10]. In the case where the stagger angle $\gamma = 0^o$, which is applicable to the case of the Wells turbine, Weinig gives the interference factor as:

$$k_0 = \frac{2s}{\pi c}\tan\left(\frac{\pi c}{2s}\right) \qquad (2)$$

Equation (2) has been extensively used by researchers as the correction factor to modify the lift coefficient of fixed-pitch Wells turbine blades. It should be noted that Weinig's theory indicates that the interference factor is predicted to be a function only of solidity and independent of angle of attack, α. However, there has previously been very little, if any, validation of this relationship for practical aerofoil cascades. The present authors have compared the inviscid flow results of (2) for a 2D linear and infinite cascade of NACA0012 aerofoils (with a stagger angle of 0º) with CFD simulations using the ANSYS CFX code. All CFD results have been obtained on a personal computer having the following hardware specification: Intel (R) Core 2CPU 6700@2.66GHz and 2.6 GHz. 2.99GB of RAM. For all simulations reported in this paper the CFX solver was run using the k-ε turbulence model with the "high resolution" advection scheme and "auto timescale". The CFD results of interference factor as a function of the inverse of solidity, s/c, and the mean angle of incidence, α_m, are presented in Fig. 4.

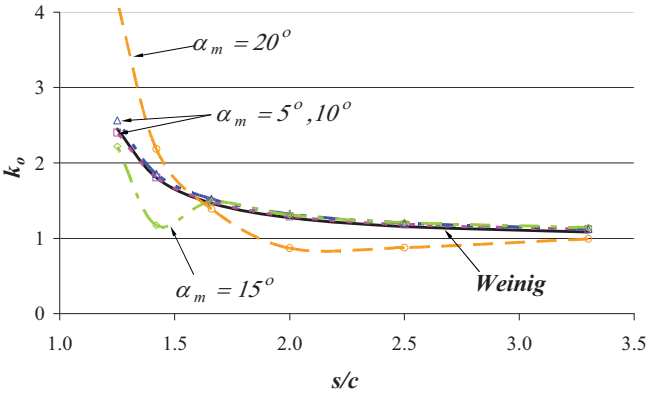

Figure 4: Lift coefficient interference factor (k_0) for a linear tandem cascade ($\gamma = 0^o$) of NACA0012 aerofoils as a function of s/c and the mean angle of incidence, α_m: □ 5º; Δ 10º; ◊ 15º; ○ 20º. Broken lines - CFD analysis; solid line – Weinig's inviscid flow analysis, eqn. (2).

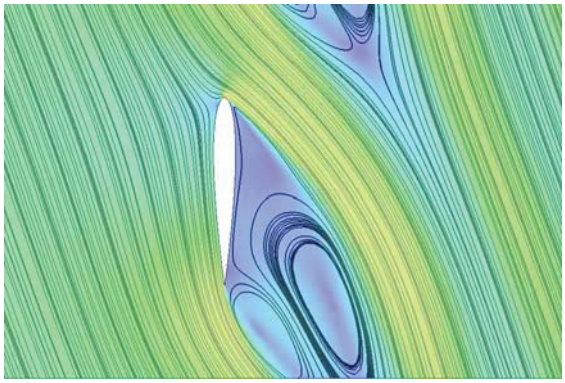

Figure 5: CFD prediction of streamlines in a tandem cascade ($\gamma = 0^o$) with $s/c=2$ and $\alpha_m = 20^o$.

The 2D simulations were carried out at Re = 7×10^5 with an unstructured grid of ~2.0 x 10^6 elements. The average cpu time for each run was about 1 hour. It is seen from Fig. 4 that there was generally good agreement between Eqn. (2) and the CFD results for small angles of attack. However, the agreement is not good for $\alpha_m > 10^o$ as a result of the inviscid flow theory not predicting the onset of stall, i.e. the CFD results show lower values of k_0 than Weinig's results due to stall and the formation of a separation region on the suction side of the aerofoil which is not accounted for in Weinig's inviscid flow analysis (Fig. 5). However for high solidity cascades (low s/c) the interference effect between adjacent blades suppresses this separation region resulting in a steep rise in cascade lift coefficient and hence an increased interference factor. The blockage effect on the pressure side is demonstrated in Fig. 6. For blades of finite thickness, small values of s/c lead to an increase in velocity in the passages and an increase in lift.

a)

b)

Figure 6: Pressure distribution for: a) s/c=1.25 and b) s/c=2 at $\alpha_m = 20^o$.

A further comparison, using a different cascade geometry, of the interference factor k_0 predicted from Weinig's inviscid flow analysis (as shown in Fig. 3) with those of a fully viscous flow CFD analysis has been conducted on a cascade of blades with the same dimensions and pitch as the scale model of the Denniss-Auld axial flow, variable-pitch turbine described by Finnigan and Auld [5]. The blade profile used for this prototype turbine was based on the NACA 65-418 with maximum camber height of 6% and maximum thickness to chord ratio of 18%. The blade geometry was symmetric about the mid-chord and was formed by combining two front halves of the NACA 65-418. Values of lift interference factor k_0 deduced from the CFD simulations for a constant upstream angle of attack $\alpha = (\beta - \gamma) = 10^o$ as a function of stagger angle and solidity is shown in Fig. 7. The results for the drag interference factor $\delta_0 = C_D/C_{D0}$ for the same cascade are also shown in Fig. 8. Two-dimensional CFD simulations have been carried out by using an unstructured mesh having a total number of elements of between 1.2 to 1.45 million depending on the stagger angle. Cascade flow was modelled using the k-ε turbulence model. The average cpu time for each run was about 55 minutes. Note that the lift and drag coefficients for the cascades have been calculated using the mean of the upstream and downstream angles of incidence as defined by Weinig [10].

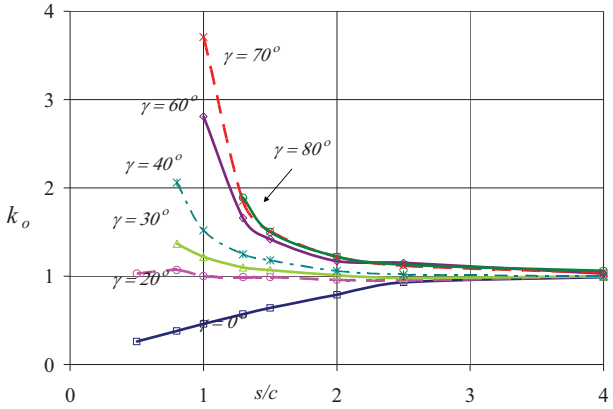

Figure 7: CFD predictions of lift interference factor for linear cascade of blades similar to those of [5] for an upstream angle of incidence $\alpha = 10^o$.

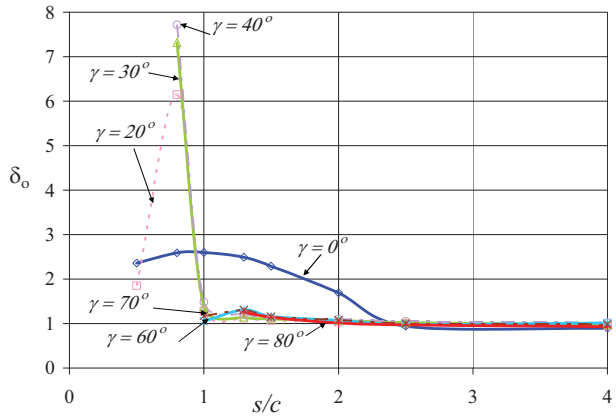

Figure 8: Interference factor for drag, δ_0, complimenting the results shown in Fig. 5. Note in this figure γ is measured from the plane normal to the plane of rotation.

The CFD results for k_0 in Fig. 7 show a close similarity to the Weinig inviscid flow analysis results

of Fig. 3 although the magnitudes of k_0 predicted from the CFD analysis are somewhat larger than Weinig's results (for $s/c < 1.5$) possibly due to the increase in velocity around the aerofoils due to the blockage effect from the finite thickness of the practical aerofoils. Note that the latter also leads to a lower limit to the value of s/c that can be implemented with practical aerofoils.

The results for the drag interference factor as a function of stagger angle and solidity shown in Fig. 8, demonstrate a trend of increasing interference factor, δ_0, with decreasing spacing of the blades. This behaviour is to be expected. It should be noted that this increase is not only the result of the effect of the neighbouring blades but also that increasing solidity results in increased restriction of the axial flow of fluid through the cascade and thus pressure drop (and hence effective drag) increases rapidly as the width of the passages between the blades fall below one chord length.

One of the few sets of experimental data showing the mutual interference between NACA0021 aerofoils in tandem cascades of three and five blades was reported by Raghunathan [10]. The present authors have simulated a linear cascade of NACA0021 aerofoils staggered at 0º using the same solidity of $\sigma = 0.5$ and with a comparable Reynolds number of 2.5×10^5 (see Fig. 9). The total number of unstructured elements in the mesh was ~ 2.3 x 10^6.

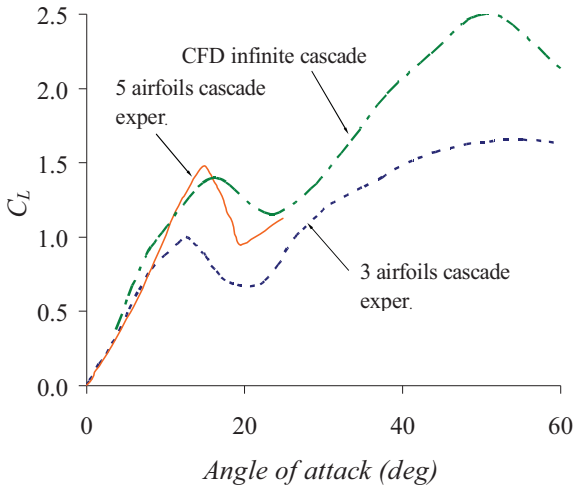

Figure 9: Comparison of experimental data for cascades of three and five NACA0021 aerofoils [10] with a CFD simulation from the present work for an infinite cascade (σ = 0.5)

Curran *et al.* [13] published lift and drag characteristics for the blades in a monoplane Wells turbine having a NACA0012 blade profile, rotor solidity of $\sigma = 0.64$ and for a Reynolds number of Re = 5.5×10^5. These lift and drag data appear to have been estimated from the turbine performance such that any swirl at the rotor was not taken into account. We have carried out 2D CFD simulations of airflow in a 2D linear rotor with the same dimensions and Reynolds numbers. The unstructured mesh used a total of ~1.6 x 10^6 elements and the cpu time for each run was between 35 to 55 minutes depending on the flow angle. The CFD and experimental lift and drag results are compared in Figs. 10 and 11 together with isolated aerofoil lift/drag data for the NACA0012 profile [14]. It is clearly seen that CFD lift results are in good agreement with lift values from [13] up to the onset of stall, which is also predicted reasonably well by the CFD analysis. The CFD analysis shows that stall occurs at a mean-span angle of attack of approximately 15º. This is opposed to a stall angle of 12º for the isolated airfoil. However, the results of Curran *et al*. do not demonstrate such a distinct onset of stall as in our CFD simulation

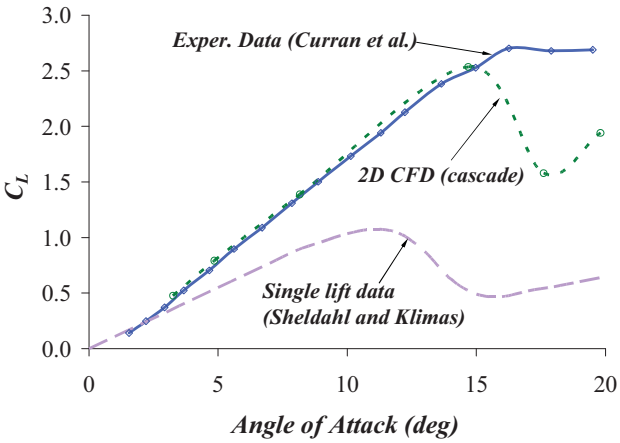

Figure 10: Comparison of lift coefficients deduced from CFD analysis and experimental rotor tests [13] for a Wells monoplane turbine with NACA0012 blade profile (σ=0.64). Isolated aerofoil lift data are also provided [14].

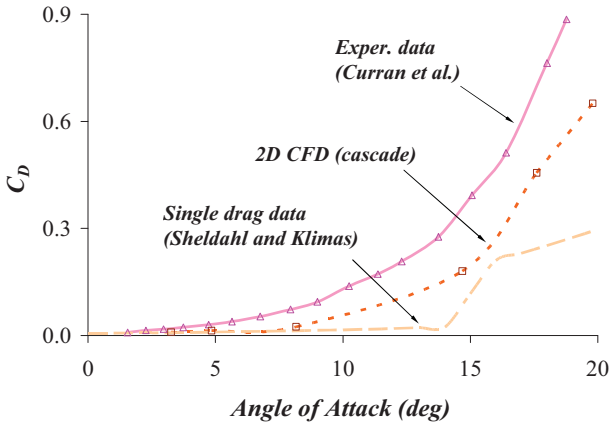

Figure 11: Comparison of drag coefficients (for same conditions as in Fig. 10).

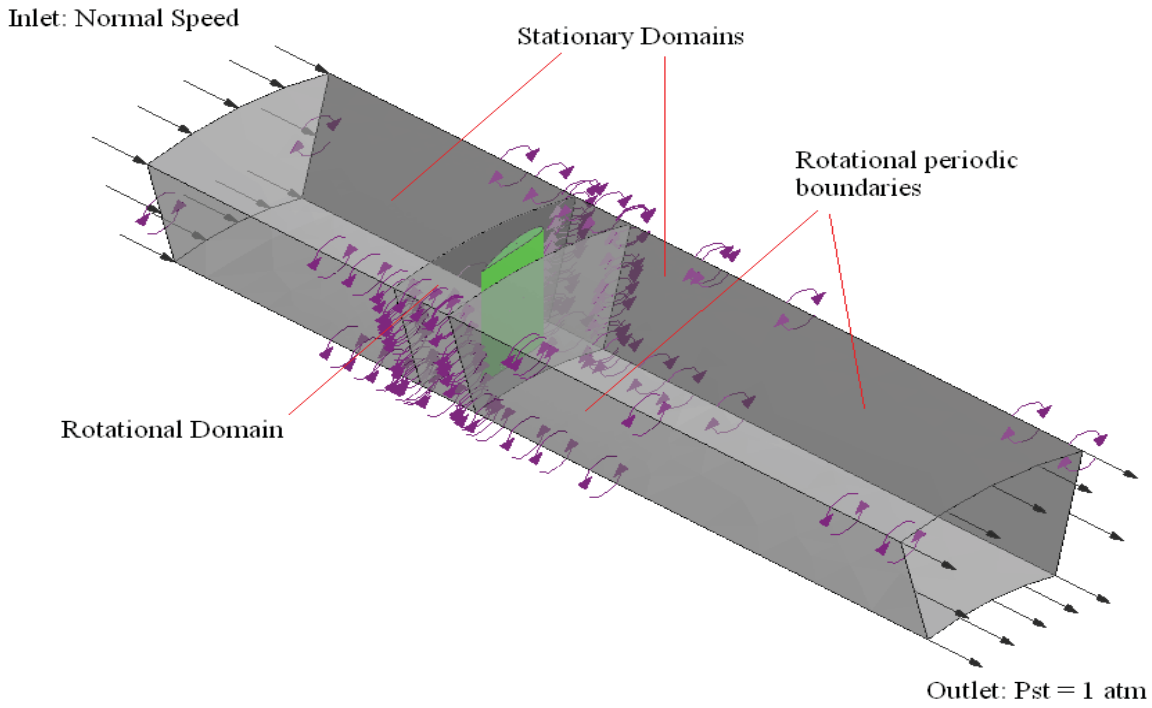

Figure 12: Computational domain of the Wells turbine with blade stagger angle, $\gamma = 3^o$.

In Fig. 11 the rotor drag coefficients obtained from the CFD analysis are shown to be lower than those reported by Curran *et al.* [13]. This less favourable agreement can be attributed to the fact that that the 2D CFD results do not include effects of aerodynamic and mechanical losses or the effects of tip clearance. However, for $3^o < \alpha < 8^o$, the CFD drag coefficients appear to be comparable to that of a single isolated aerofoil.

3 Three-Dimensional CFD Rotor Analysis

One of the goals of the present research was to investigate the utility of 3D CFD simulations of axial flow turbines designed to service OWC wave energy converters. A CFD simulation of a variable pitch Wells turbine was carried out. No-slip boundary conditions were specified at the blade surface, hub, rotor and shroud and rotational periodicity was applied along the meridian surfaces for each of the thirteen blades (Fig. 12).

To model airflows through this type of turbine, one of the first and most important steps is to replicate the blade geometry and to develop a grid with appropriate topology/resolution, particularly in the vicinity of blade. Both structured and unstructured meshes have been investigated in the present study. A total of ~10^6 elements were used in the structured grids for large stagger angles ($\gamma = 24^o$, and $\gamma = 32^o$). For smaller angles ($\gamma = 3^o$, $\gamma = 11^o$) and blades staggered at 0^o an unstructured mesh was employed with a total number of elements of ~2.6 x 10^6. For each 3D CFD run the cpu time was about 2 hrs. A typical example of a structured mesh with a blade stagger angle of $\gamma = 32^o$ is illustrated in Fig. 13.

Torque, input, and pressure coefficients are defined as follows.

$$C_t = \frac{Torque}{\rho\left(V_z^2 + (\Omega R_{av})^2\right) b\, c\, \mathrm{N} R_{av}/2} \qquad (4)$$

$$C_a = \frac{\Delta p Q}{\rho\left(V_z^2 + (\Omega R_{av})^2\right) b\, c\, \mathrm{N} V_z/2} \qquad (5)$$

$$P^* = \frac{\Delta p}{\rho \Omega^2 R_{av}^2} \qquad (6)$$

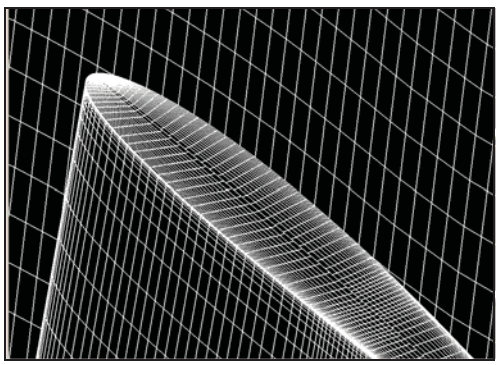

Figure 13: Typical example of a structured mesh on the blade surface for $\gamma = 32^o$.

A comparison of experimental and CFD data published by Torresi *et al.* [15] with our 3D CFD simulations for non-dimensional pressure coefficient, P^*, is shown in Fig. 14, where good agreement is demonstrated.

The results reported by Tease [16], as part of the Wavegen Variable Pitch Wells Turbine research program, have provided valuable information for possible verification of our 3D CFD results. Experimental and CFD values of non-dimensional pressure coefficient, P^*, as a function of flow factor, ϕ, for different blade stagger angles, γ, are shown in Fig. 15. It is evident that the CFD results provide a reasonably good match to the experimental data.

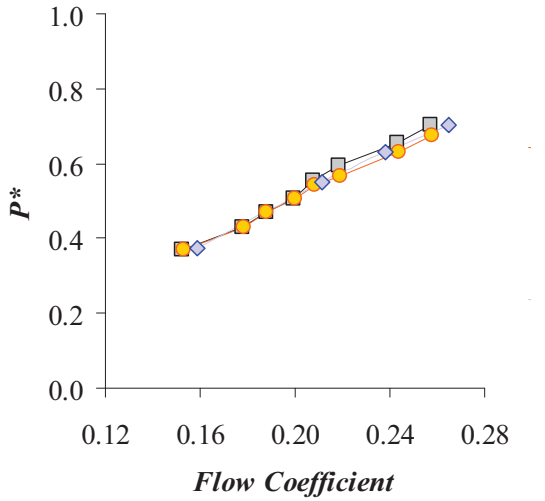

Figure 14: Comparison of P^* for the Wells turbine studied in [15]: ◊ – CFD results of present authors; □ – experimental and ○ – CFD results of Torresi *et al.* [15].

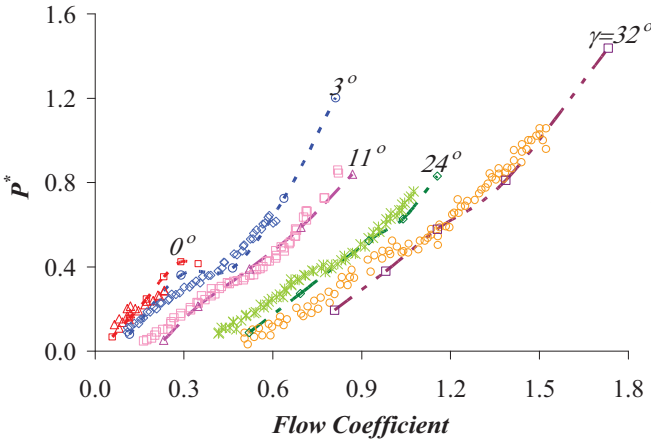

Figure 15: Comparison experimental results illustrating variation of the rotor non-dimensional pressure (symbols) with flow factor for different blade stagger angles [16] and P^* deduced from present 3D CFD simulations (broken lines).

4 Comparison of 3D CFD and Blade Element Analysis

Cooper and Gareev [17] reported the development of a non-dimensional blade-element model for axial flow turbines. They determined that by recasting the blade element/actuator disk equations in non-dimensional form the performance of an axial flow turbine may be expressed as a function of only non-dimensional parameters in the following form.

$$C_T = \frac{4\pi\phi a'(R_t + R_r)}{(\phi^2+1)Nc} = \frac{4\phi a'}{(\phi^2+1)\sigma} \qquad (7)$$

$$C_a = \frac{(\phi^2 + (1+a')^2)C_\theta}{\phi^2+1} = \frac{2P^*}{\sigma(\phi^2+1)} \qquad (8)$$

$$P^* = \sigma C_\theta\left(\phi^2 + (1+a')^2\right)/2 \qquad (9)$$

$$\eta = 2a'/P^* \qquad (10)$$

Here solidity, σ= c/s, tangential induction factor, $a' = V_\theta/(\Omega R)$, flow factor, $\phi = V_z/V_\theta$ and C_ϕ and C_θ are the blade axial and tangential force coefficients, respectively, which, using the present nomenclature of Fig. 2, are expressed as:

$$C_\phi = C_L \cos\beta + C_D \sin\beta \qquad (11)$$

$$C_\theta = C_L \sin\beta - C_D \cos\beta \qquad (12)$$

The non-dimensional form of the tangential induction factor, a', is given as:

$$a' = \frac{[\phi^2 + (1+a')^2]\sigma C_\phi}{4\phi} \qquad (13)$$

In the present work we have compared the CFD results with the non-dimensional blade element model, equations (7) to (13), in terms of torque coefficient, C_t, and pressure coefficient, P^*, with a view to assessing the robustness of the blade element model. The situation modelled was that of the Wells turbine tested by Tease [16]. The lift and drag coefficients, C_L and C_D, used in the blade element model were determined from our 2D CFD cascade analysis and are shown in Fig. 16. The agreement between the CFD and blade element analyses is generally good. At a stagger angle of 24° the simulated flow factor ranged from 0.52 to 1.16 which corresponded to angles of attack of 3.5° to 25°. At a stagger angle of 32° the simulated flow factor ranged from 0.81 to 1.73 which corresponded to angles of attack of 7° to 28° At these two stagger angles both the CFD and blade element model indicate that mild stall occurrs at flow factors of 1.05 and 1.2, respectively. At a stagger angle of 11° the blade element model clearly predicts stall at a flow factor of 0.6 whereas the CFD only predicts a mild onset of stall. In general, the CFD simulations predict milder stall compared to the blade element momentum model due to the three-dimensional flow effects within the cylindrical cascade of the real rotor.

A plot of torque coefficient, C_t, as a function of flow factor ϕ, as deduced from 3D CFD simulations of the Wells turbine of Tease [16] is shown in Fig. 17. It is

clearly seen that increasing the blade stagger angle of the Wells turbine leads to an increase in the flow factor at which the onset of stall occurs and also leads to an increase in the magnitude of the torque coefficient, C_t. The trend can be explained by the decrease in the angle of attack angle when the stagger angles increase. Similar data for C_t is also obtained using the blade element model and the two are compared in Fig. 18. Although the general form of the results is qualitatively the same, there are significant quantitative differences which suggest that the blade element model does not capture important 3D aspects of the flow in the rotor.

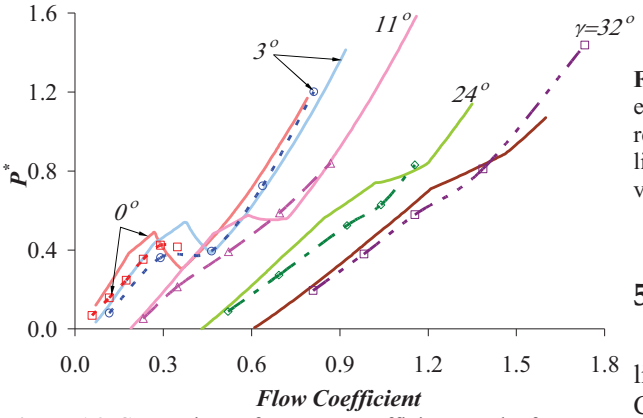

Figure 16: Comparison of pressure coefficient results from the blade element model (symbols/broken lines) and from 3D CFD simulations (continuous lines), for the geometry of the variable pitch angle Wells turbine described by Tease [16].

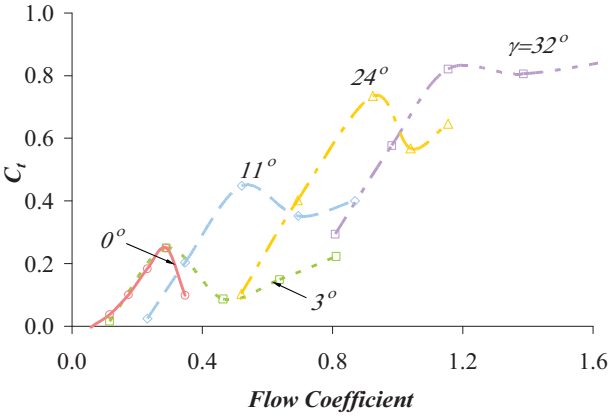

Figure 17: Variation of torque coefficient C_t from 3D CFD simulations of a variable pitch angles Wells turbine [16].

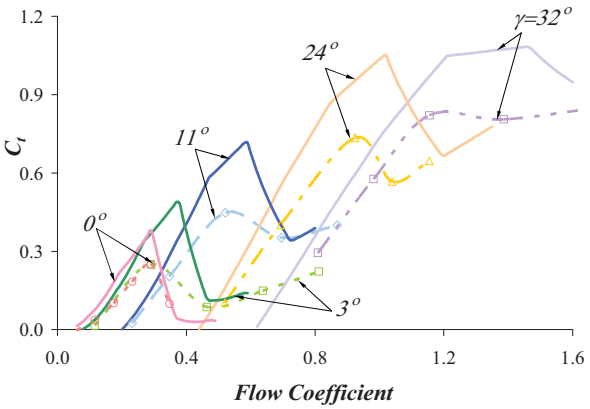

Figure 18: Comparison numerical results based on a blade element model and cascade lift/drag data (symbols) against results for C_t deduced from 3D CFD simulations (broken lines). Both set of data obtained by present authors for a variable pitch (stagger) angles Wells turbine prototype [16].

5 Conclusions

An analysis of the lift and drag characteristics of linear cascades of aerofoils was performed using Computational Fluid Dynamics (CFD). The CFD methodology was used to generate interference factors that facilitate the use of lift and drag coefficients from isolated aerofoil data in blade element/actuator disc models of air turbines in OWCs.

The CFD analysis has demonstrated that for angles of attack such that $\alpha \leq 10°$ Weinig's inviscid flow analysis provides an accurate prediction of the interference factor for lift, k_0. Weinig's analysis did not account for the finite thickness of practical blades in a cascade, and our CFD results indicate a higher interference factor for high values of rotor solidity because of higher air velocities within the blade passages than would occur for blades of zero thickness. The results of the CFD analysis of the effective drag interference factors, δ_0, for a cascade are also presented.

We have demonstrated that single aerofoil data and interference factors may be used effectively in blade element/actuator disk analysis of a variable pitch Wells turbine. Our blade element results have been compared to both the original experimental results of Tease [16] and with the full 3D CFD simulations of the present study. Comparison of the data shows that the blade element results and CFD match the non-dimensional pressure experimental data well, however the match in the case of the torque coefficient is less precise.

References

[1] T.J.T Whittaker, W. Beattie, M. Folley, C. Boake, A. Wright, M. Osterried, and T. Heath. Performance of the LIMPET Wave Power Plant – Prediction, Measurement and Potential, *5th European Wave Energy Conf.*, Cork, paper FS5, 2003.

[2] A. Brito-Melo, F. Neuman, and A.J.N.A Sarmento, Full-scale data assessment in OWC Pico plant, *Int. J. Offshore and Polar Engineering,* 18:27-34, 2008

[3] Oceanlinx (2008) http://www.oceanlinx.com/ accessed 15/4/2009.

[4] A.A. Wells. Fluid driven rotary transducer, *British Patent no. 1 595 700*, 1976

[5] T. Finnigan. and D. Auld. Model Testing of a Variable-Pitch Aerodynamic Turbine. *Proc. Int. Offshore and Polar Engineering Conf.*, 357-360, 2003.

[6] G. Thomas. The theory behind the conversion of ocean wave energy: A review, in *Ocean wave Energy: Current Status and Future Perspectives*, edit Cruz, C., Springer, Berlin, 2008.

[7] S. L. Dixon. Fluid mechanics, thermodynamics of turbomachinery. Pergamon, 1975.

[8] S. Raghunathan. The Wells Air Turbine for Wave Energy *Conversion. Prog. Aerospace Sci*., 31:335-386, 1995.

[9] F.S. Weinig. Theory of two-dimensional flow through cascades (in *Aerodynamics of turbines and compressors*, volume X, edit. Hawthorne, W.R., Princeton University Press, 13-81, 1964.

[10] S. Ragunathan. Aerodynamics forces on aerofoils at high angles of attack, *AIAA Nat. Fluid Dynamics Congress*, pap. 88-3697, Cincinnati, USA, 1710-1717, 1988.

[11] W.R Hawthorne and J.H. Horlock. Actuator disc theory of the incompressible flow in axial compressors. *Proc. Inst. Mech. Engrs.*, 176:789, 1962

[12] L.M.C. Gato and A. F. de O. Falcão. On the Theory of the Wells Turbine. *ASME J. Engineering for Gas Turbines and Power*, 106:628-633, 1984.

[13] R. Curran, T.J.T Whittaker, S. Raghunathan, W.C. Beattie. Performance Prediction of Contra-rotating Wells Turbines for Wave Energy Converter Design. *Journal of Energy Engineering*, 124, 1998.

[14] R. E. Sheldahl and P. Klimas. *Aerodynamic characteristics of Seven Symmetrical Aerofoil Sections Through 180-Degree Angle of Attack for Use in Aerodynamic Analysis of Vertical Axis Wind Turbines*, Sandia National Laboratories report, SAND80-2114, 1981.

[15] M. Torresi, S. M. Camporeale, and G. Pascazio. Experimental and numerical investigation on the performance of a Wells turbine prototype. *Proc. 7th European Wave and Tidal Energy Conference*, Porto, Portugal, 2007.

[16] W. K. Tease. Dynamic Response of a Variable Pitch Wells Turbine. *Proc. 5th European Wave Energy Conf.*, Cork, Ireland, September 2003.

[17] P. Cooper and A. Gareev. Numerical analysis of a variable pitch reversible flow air turbine for oscillating water column wave energy systems. In Proc 7th European Wave and Tidal Energy Conference, EWTEC, Portugal, 2007.